First-principles calculations of phase transition, low elastic modulus, and superconductivity for zirconium

Bao-Tian Wang,[1, 2, ∗] Peng Zhang,[3] Han-Yu Liu,[4] Wei-Dong Li,[1] and Ping Zhang[2, 5, †]

[1]*Institute of Theoretical Physics and Department of Physics,*

Shanxi University, Taiyuan 030006, People's Republic of China

[2]*LCP, Institute of Applied Physics and Computational Mathematics,*

P.O. Box 8009, Beijing 100088, People's Republic of China

[3]*Department of Nuclear Science and Technology,*

Xi'an Jiaotong University, Xi'an 710049, People's Republic of China

[4]*State Key Lab of Superhard Materials, Jilin University,*

Changchun 130012, People's Republic of China

[5]*Center for Applied Physics and Technology,*

Peking University, Beijing 100871, People's Republic of China

Abstract

The elasticity, dynamic properties, and superconductivity of α, ω, and β Zr are investigated by using first-principles methods. Our calculated elastic constants, elastic moduli, and Debye temperatures of α and ω phases are in excellent agreement with experiments. Electron-phonon coupling constant λ and electronic density of states at the Fermi level $N(E_{\mathrm{F}})$ are found to increase with pressure for these two hexagonal structures. For cubic β phase, the critical pressure for mechanical stability is predicted to be 3.13 GPa and at P=4 GPa the low elastic modulus (E=31.97 GPa) can be obtained. Besides, the critical pressure for dynamic stability of β phase is achieved by phonon dispersion calculations to be ∼26 GPa. Over this pressure, λ and $N(E_{\mathrm{F}})$ of β phase decrease upon further compression. Our calculations show that the large value of superconducting transition temperature T_{c} at 30 GPa for β Zr is mainly due to the TA1 soft mode. Under further compression, the soft vibrational mode will gradually fade away.

PACS numbers: 62.20.Dc, 64.70.kd, 61.50.Ks, 74.70.Ad

∗E-mail: wbt11129@sxu.edu.cn

†Corresponding author; zhang_ping@iapcm.ac.cn

I. INTRODUCTION

Group IV transition metals such as titanium, zirconium, and hafnium have wide applications in the aerospace, nuclear, and biomedical industry [1–3]. The body-centered cubic (bcc) type (β phase) of Ti and Zr alloys in usage as metallic biomaterial have been studied extensively because of their properties of nontoxicity, high strength, good biocompatibility, and low elastic modulus [1, 4]. However, the investigations of the single crystal β Zr as biomaterial has not been reported.

Actually, at ambient condition Zr crystallizes in hexagonal closed-packed (hcp) structure (α phase). And at high temperature of 1135 K, it transforms into the β phase. At room temperature and under pressure range of 2-7 GPa [5–7], the α phase transforms to another more open hexagonal structure of ω phase with space group $P6/mmm$ (No. 191). And under further high pressure of 30-35 GPa, the $\omega{\to}\beta$ phase transition has been observed [6, 8–11]. The Young's moduli of both α and ω phases at ambient condition are largely bigger than that of a human bone (about 30 GPa). So the condition of low elastic modulus cannot be satisfied for these two phases. As for β phase, it cannot be exploited because the reverse phase transformations take place upon unloading. So it seems that we should not consider metal Zr as candidate biomaterial. But, fortunately recent experiment has successfully stabilized the β Zr at room temperature using compression stresses higher than 3 GPa plus the controlled application of shear [3]. This makes stabilizing the high temperature or pressure phases of Zr at ambient conditions reality. Therefore, the study of the elastic modulus for β Zr at low pressure is valuable.

As another key objective of our work, we calculate the superconducting transition temperature T_c for metal Zr. Although the T_c of Zr has been observed in experiments [9], to date no theoretical work is found in the literature. Our calculations will show that the increase (decrease) in T_c with pressure can be understood in terms of the enhancement (reduction) of the electronic density of states (DOS) at the Fermi level and the corresponding behaviors of electron-phonon coupling constant. In present study, the dynamic stability of β Zr is tested carefully by performing phonon dispersion calculations. The $\beta{\to}\omega$ and $\beta{\to}\alpha$ transitions are discussed in detail. The rest of this paper is arranged as follows. In Sec. II the computational methods are described. In Sec. III we present and discuss our results. In Sec. IV we summarize the conclusions of this work.

II.   COMPUTATIONAL METHODS

A.   Computational details

The first-principles density functional theory (DFT) calculations on the basis of the frozen-core projected augmented wave (PAW) method of Blöchl [12] are performed within the Vienna *ab initio* simulation package (VASP) [13], where the Perdew, Burke, and Ernzerhof (PBE) [14] form of the generalized gradient approximation (GGA) is employed to describe electron exchange and correlation. For the plane-wave set, a cutoff energy of 500 eV is used. The Γ-centered k point-meshes in the full wedge of the Brillouin zone (BZ) are sampled by 18×18×16, 16×16×18, and 18×18×18 grids according to the Monkhorst-Pack (MP) [15] for α (two-atom cell), ω (three-atom cell), and β (two-atom cell) Zr, respectively, and all atoms are fully relaxed until the Hellmann-Feynman forces become less than 0.001 eV/Å. The Zr $4d^35s^1$ orbitals are explicitly included as valence electrons. The pseudopotential plane-wave method within the PBE-GGA through the QUANTUM-ESPRESSO package [16] is employed to calculate the electronic properties, lattice dynamics, and electron-phonon coupling (EPC) for Zr, where the Zr $4s^24p^64d^25s^2$ are treated as valence electrons. Convergence tests give the choice of kinetic energy cutoffs of 60 Ry with Gaussians width of 0.05 Ry for all three phases of Zr and 12×12×8, 8×8×12, and 16×16×16 MP grids of k-point meshes for α, ω, and β Zr, respectively. Phonon frequencies are calculated based on the density functional linear-response method [17, 18]. In the interpolation of the force constants for the phonon dispersion curve calculations, 6×6×4, 4×4×6, and 8×8×8 q-point meshes and denser 24×24×16, 16×16×24, and 32×32×32 k-point meshes in the first BZ are used for α, ω, and β phases of Zr, respectively.

B.   Mechanical properties

To avoid the Pulay stress problem, the geometry optimization at each volume is performed at fixed volume rather than constant pressure. The theoretical equilibrium volume, bulk modulus B, and pressure derivative of the bulk modulus B' are obtained by fitting the energy-volume data in the third-order Birch-Murnaghan equation of state (EOS) [19]. Elastic constants for cubic symmetry (C_{11}, C_{12}, and C_{44}) and hexagonal structure (C_{11}, C_{12}, C_{13}, C_{33}, and C_{44}) are calculated by applying stress tensors with various small strains

onto the equilibrium structures. The strain amplitude δ is varied in steps of 0.006 from $\delta=-0.036$ to 0.036. After obtaining elastic constants, the polycrystalline bulk modulus B and shear modulus G are calculated from the Voigt-Reuss-Hill (VRH) approximations [20]. The Young's modulus E and Poisson's ratio υ are calculated through $E = 9BG/(3B+G)$ and $\upsilon = (3B-2G)/[2(3B+G)]$. In calculation of the Debye temperature (θ_D), we use the relation

$$\theta_D = \frac{h}{k_B}\left(\frac{3n}{4\pi\Omega}\right)^{1/3}\upsilon_m, \tag{1}$$

where h and k_B are Planck and Boltzmann constants, respectively, n is the number of atoms in the molecule, Ω is molecular volume, and υ_m is the average sound wave velocity. The average wave velocity in the polycrystalline materials is approximately given as

$$\upsilon_m = \left[\frac{1}{3}\left(\frac{2}{\upsilon_t^3}+\frac{1}{\upsilon_l^3}\right)\right]^{-1/3}, \tag{2}$$

where $\upsilon_t = \sqrt{G/\rho}$ (ρ is the density) and $\upsilon_l = \sqrt{(3B+4G)/3\rho}$ are the transverse and longitudinal elastic wave velocity of the polycrystalline materials, respectively.

C.   Superconduntivity

The superconducting transition temperature T_c is evaluated by using the Allen-Dynes modified McMillan equation [21, 22]

$$T_c = \frac{\omega_{\log}}{1.2}\exp\left[-\frac{1.04(1+\lambda)}{\lambda-\mu^*(1+0.62\lambda)}\right], \tag{3}$$

where

$$\omega_{\log} = \exp\left[\frac{2}{\lambda}\int_0^\infty \frac{d\omega}{\omega}\alpha^2 F(\omega)\ln\omega\right] \tag{4}$$

is the logarithmic average frequency,

$$\lambda = 2\int_0^\infty \frac{\alpha^2 F(\omega)}{\omega}d\omega \tag{5}$$

is the electron-phonon coupling constant, and μ^* is the Coulomb pseudopotential. The Eliashberg electron-phonon spectral function $\alpha^2 F(\omega)$ is written as

$$\alpha^2 F(\omega) = \frac{1}{2\pi N(E_F)}\sum_{qv}\frac{\gamma_{qv}}{\omega_{qv}}\delta(\omega-\omega_{qv}), \tag{6}$$

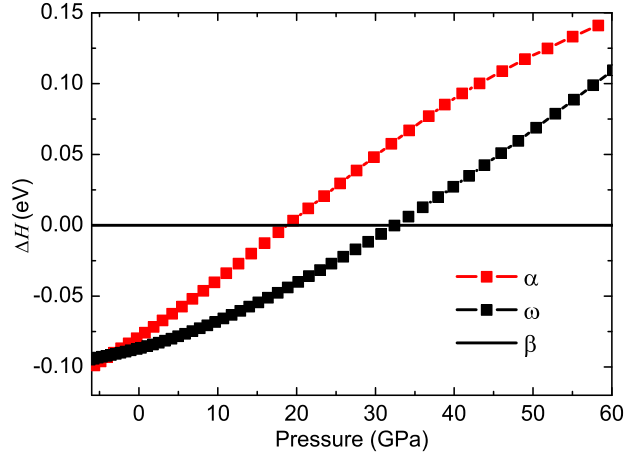where $N(E_F)$ is the electronic density of state (DOS) at the Fermi level.

FIG. 1: (Color online) Calculated enthalpy differences of α and ω phases with respect to β phase as functions of pressure.

III. RESULTS

At 0 K, the Gibbs free energy is equal to the enthalpy H. After calculation, we can plot in Fig. 1 the relative enthalpies of the α and the ω phases with respect to the β phase as functions of pressure. The crossing between the α and ω enthalpy curves readily gives phase transition pressure of -3.7 GPa, which indicates that at ambient pressure the ω phase is more stable than the α phase. This fact is in disagreement with experiment, but coincides well with recent DFT-PBE [23] and FP-LAPW [24] calculations. The disagreement between theory and experiment mainly originates from temperature effect. Actually, previous DFT-PBE [23] study clearly shows that the transition of $\alpha \rightarrow \omega$ occurs at 1.7 GPa at T=300 K. As for the $\omega \rightarrow \beta$ transition, a pressure of 32.4 GPa is obtained. This value falls exactly in the pressure range of $30-35$ GPa measured by experiments [6, 8–11] and also fairly accords with other calculations [23, 24].

In Table I, we report our calculated lattice parameters, bulk modulus, pressure derivative of the bulk modulus, and elastic constants of α, ω, and β Zr at different pressures. For comparison, the experimental values [2, 7, 25–27] and other theoretical results [1, 28, 29] are also listed. Obviously, our calculated results accord well with experiments and other calculations for α and ω phases. However, for β Zr the difference of lattice parameter and bulk modulus between our calculation and the experiment from Zhao *et al.* [7] is evident. This is due to the fact that the experiment is conducted at T=973 K, while our calculation

5

TABLE I: Calculated lattice parameters (a or c), bulk modulus (B), pressure derivative of the bulk modulus (B'), and elastic constants of α, ω, and β Zr at different pressures. For comparison, experimental values and other theoretical results are also listed.

Phase	Method	Pressure (GPa)	a (Å)	c (Å)	B (GPa)	B'	C_{11} (GPa)	C_{12} (GPa)	C_{13} (GPa)	C_{33} (GPa)	C_{44} (GPa)
α	This work	0	3.236	5.168	96.0	3.12	146.7	68.5	71.0	163.3	26.0
		5.35	3.178	5.093			162.3	78.4	81.9	187.5	24.9
	DFT-PBE[a]	0	3.240	5.178	93.4	3.22	141.1	67.6	64.3	166.9	25.8
	DFT-PBE[b]	0	3.232	5.182	93.4	3.22	139.4	71.3	66.3	162.7	25.5
	Expt.	0	3.233[c]	5.146[c]	92[c]	4.0[c]	144.0[d]	74.0[d]	67.0[d]	166.0[d]	33.0[d]
ω	This work	0	5.036	3.152	96.9	3.39	161.7	72.6	53.5	195.6	33.7
		6.04	4.939	3.097			187.0	85.8	63.1	224.4	37.3
		10.01	4.884	3.066			201.5	94.5	69.0	241.1	38.8
	DFT-PBE[a]	0	5.056	3.150	101.1	3.27	165.2	75.6	47.5	198.7	30.6
	Expt.	0	5.039[e]	3.150[e]	104.0[f]	2.8[f]					
β	This work	0	3.574		90.2	3.06	86.6	92.3			26.6
		10	3.461				123.1	106.6			32.0
		20	3.374				160.0	116.8			37.0
		30	3.302				196.9	124.1			42.2
		35	3.271				216.7	124.4			45.8
		40	3.241				235.2	128.4			49.2
		50	3.188				265.6	136.2			54.4
		60	3.141				298.3	141.3			61.7
	DFT-PBE[b]	0	3.580				84.2	91.4			32.3
	LDA[g]	0									32.8
	Expt.	0	3.627[c]		66[c]		104[h]	93[h]			38[h]

[a] Reference [28], [b] Reference [1], [c] Reference [7], [d] Reference [27], [e] Reference [25], [f] Reference [2], [g] Reference [29], [h] Results measured at T=915°C from reference [26].
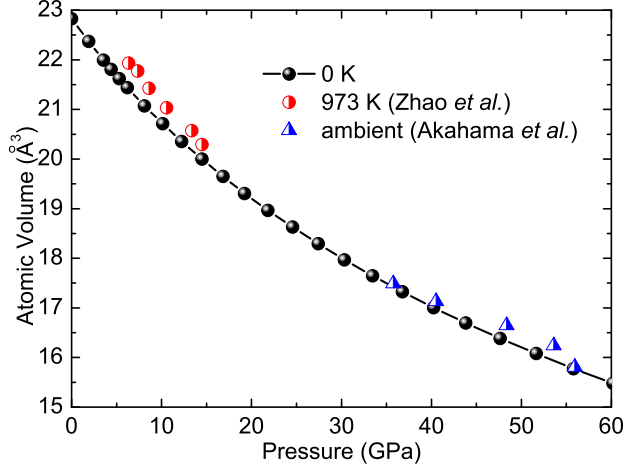
FIG. 2: (Color online) Calculated compression curves of β Zr compared with experimental measurements.

is valid only at 0 K. Similar temperature effect for β Zr is also found in studying the compression behaviour. As shown in Fig. 2, although good consistence with the experiment [10] at high pressure domain is clear, the values of the atomic volumes are smaller than that by experiment at T=973 K. Nevertheless, the compression performance of β Zr is wholly consistent with experiments. From Table I, one can find that the difference of elastic constants at zero pressure between calculation and experiment is evident. This also can be attributed to the temperature effect. In fact, the good accordance of the lattice parameter and elastic constants of β Zr at 0 GPa between our calculation and previous DFT-PBE [1] study supplies the safeguard for our study of structure, mechanical, and electronic properties of β Zr. Additionally, the mechanical stability of α and ω Zr at 0 GPa and at some typical finite pressures can be predicted from the elastic constants data. But the elastic constants of β Zr at 0 GPa illustrate that the cubic phase is mechanically unstable, which is in good agreement with the results by Ahuja et $al.$ [29] and Ikehata et $al.$ [1]. Actually, the mechanical stability of β Zr can be obtained through applying external pressure and our data show that along with the increase of pressure from 0 GPa to 60 GPa, the value of $C_{11} - C_{12}$ increases almost linearly from -5.7 GPa to 157 GPa. Fitting the curve (not shown) of the pressure behaviour of $C_{11} - C_{12}$ by first-order polynomial function, we find that the value of $C_{11} - C_{12}$ becomes positive at $P \geq 3.13$ GPa. In fact, at P=4 GPa our first-principles calculated C_{11}, C_{12}, and C_{44} equal to 101.8, 98.2, and 28.7 GPa, respectively,

7

TABLE II: Calculated elastic moduli, Poisson's ratio (v), density (ρ), transverse (v_t), longitudinal (v_l), and average (v_m) sound velocities calculated from polycrystalline bulk and shear modulus, and Debye temperature of α, ω, and β Zr at different pressures. For comparison, experimental values and other theoretical results are also listed.

Phase	Method	Pressure	B	G	E	v	ρ	v_t	v_l	v_m	θ_D
		(GPa)	(GPa)	(GPa)	(GPa)		(g/cm^3)	(km/s)	(km/s)	(km/s)	(K)
α	This work	0	97.4	33.8	91.0	0.344	6.465	2.288	4.695	2.571	267.3
		5.35	110.4	34.9	94.8	0.357	6.804	2.266	4.803	2.550	269.8
	Expt.[a]	0	95.3	36.3	96.6	0.331	6.511	2.361	4.698		275.9
ω	This work	0	97.5	43.6	113.7	0.306	6.568	2.575	4.868	2.878	300.9
		6.04	113.5	49.0	128.5	0.311	6.948	2.655	5.074	2.970	276.4
		10.01	123.2	51.6	135.8	0.316	7.177	2.681	5.172	3.001	282.3
	Expt.[a]	0	104.0	45.1	118.3	0.311	6.589	2.616	4.996		306.1
		6.88						2.638	5.177		
		10.59						2.652	5.284		
β	This work	10	112.1	18.7	53.1	0.421	7.309	1.599	4.330	1.816	196.7
		20	131.2	29.8	83.2	0.394	7.889	1.944	4.655	2.199	244.4
		30	148.4	39.8	109.6	0.377	8.415	2.175	4.893	2.454	278.7
		35	156.5	45.5	124.6	0.367	8.662	2.293	5.008	2.584	296.3
		40	164.0	50.9	138.3	0.360	8.900	2.390	5.104	2.691	311.4
		50	179.3	58.3	157.8	0.353	9.353	2.497	5.243	2.809	330.4
		60	193.6	68.0	182.5	0.343	9.781	2.636	5.391	2.961	353.5
	Expt.[b]	0	96.7	18.1	51.2	0.412	6.420	1.681	4.339	1.906	197.8, 177[c]

[a] Reference [30], [b] Calculated using present scheme with elastic constants at T=915°C from reference [26], [c] Reference [26].

which explicitly indicate the elastic stability of bcc Zr under this pressure.

After obtaining elastic constants, the elastic moduli, Poisson's ratio (v), transverse sound velocities (v_t), longitudinal sound velocities (v_l), average sound velocities (v_m), and Debye temperature of α, ω, and β Zr at different pressures are calculated and tabulated in Table II. The experimental values [26, 30] are also collected in Table II for comparison. The excellent
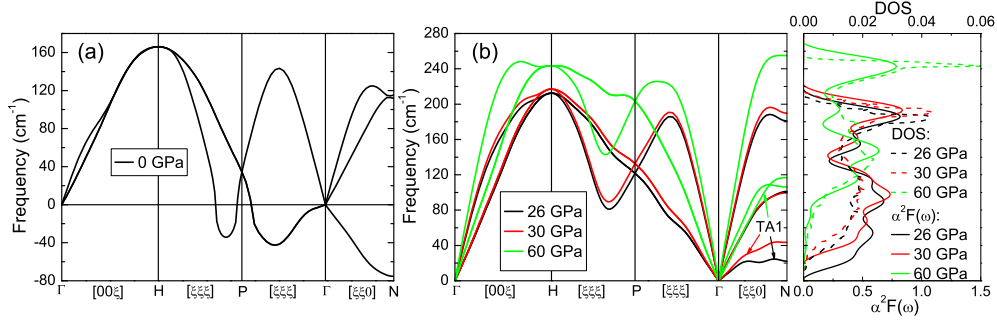
FIG. 3: (Color online) Phonon dispersion at 0 GPa (a) and phonon dispersion, Eliashberg phonon spectral function, and phonon DOS at 26, 30, and 60 GPa (b) for β Zr.

coincidence between our calculation and experiment for α and ω phases can be seen. For β phase, the bulk modulus B, shear modulus G, Young's modulus E, and Debye temperature all linearly increase with pressure. The Young's modulus E at P=4 GPa (just over the critical pressure 3.13 GPa for the elastic stability of β Zr) is calculated to equal to 31.97 GPa, which is very near the Young's modulus value ($\sim$30 GPa) of a human bone. Thus, we successfully indicate the importance of stabilizing the high temperature or pressure phase of Zr at ambient conditions. In Table II, we also list the results of β phase calculated using present scheme with elastic and lattice constants at T=915°C from Ref. [26]. The derived Debye temperature is slightly higher than that given in Ref. [26].

Phonon dispersion results for β Zr at selected pressures are shown in Fig. 3. Like the β phase of Ti and Hf [31, 32], the high pressure β phase of Zr is also dynamically unstable at low pressure [Fig. 3(a)]. Our phonon dispersion calculations at high pressure illustrate that the β Zr becomes dynamically stable at around 26 GPa. In fact, no imaginary frequencies are observed at 26-60 GPa pressure domain as clearly indicated in Fig. 3(b). Therefore, although recent experiment by Pérez-Prado and Zhilyaev [3] has successfully stabilized the high pressure/temperature phase of Zr at ambient condition, our phonon dispersion calculations illustrate that the β phase is dynamically unstable in pressure domain of 0-25 GPa at 0 K. This fact confirms that the temperature effect on the phase stability is also critical for the experimentally observed [3] β phase at ambient condition. Besides, the dynamical stability test at 26-60 GPa supplies the safeguard for our following study of the superconductivity of β Zr at high pressure. As shown in Fig. 3(a), our phonon dispersion results indicate soft modes for the longitudinal L $\frac{2}{3}$[111] and transverse T $\frac{1}{2}$[110] phonons.

9

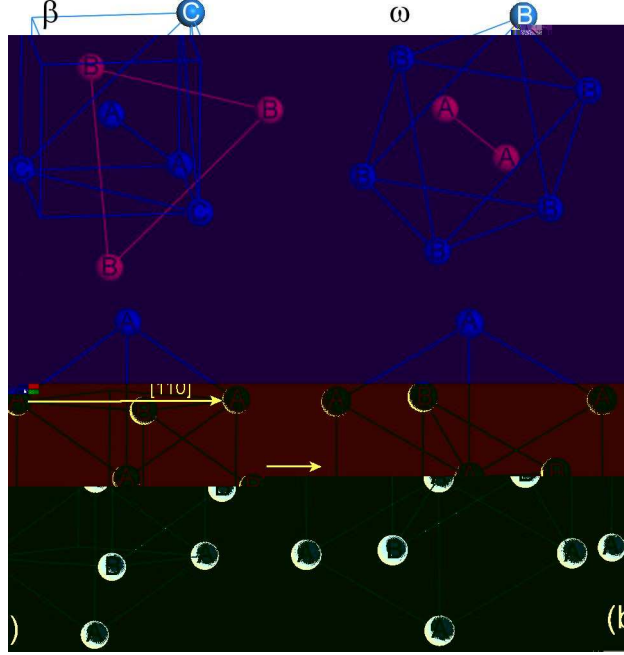FIG. 4: (Color online) Schematic illustrations of the structural transition for (a) $\beta\rightarrow\omega$ and (b) $\beta\rightarrow\alpha$.

As indicated by experiment [26], the L $\frac{2}{3}$[111] unstable phonon branch is responsible for the $\beta\rightarrow\omega$ transition and the T $\frac{1}{2}$[110] implies the $\beta\rightarrow\alpha$ transition. In Fig. 4, we show the paths of $\beta\rightarrow\omega$ and $\beta\rightarrow\alpha$ transitions. As shown in Fig. 4(a), the bcc β phase can be viewed as ABC periodically layered structure along the [111] direction and there are two periods of ABC layers in its unit cell. For ω phase, it can be viewed as AB periodical layered structure along the [0001] direction [Fig. 4(a)]. The atoms on B and C layers in β phase move easily along the soft mode direction of [111] and can transfer to be the B layer of ω phase. Therefore, the atomic displacement along the [111] direction is the main origin for the $\beta\rightarrow\omega$ phase transition. For $\beta\rightarrow\alpha$ transition, one can regard the β phase as two layered (AB) structure along the [1$\bar{1}$0] orientation [Fig. 4(b)]. In transition, firstly the atoms on each layer expand along the [110] direction to form a hexagon, and second, the adjacent (1$\bar{1}$0) planes slip relatively along the [110] direction to create the hcp structure.

For high pressure phase of Zr, it has evident predominance for high-temperature superconductivity. The EPC calculations have been performed to explore the superconductivity. The Eliashberg phonon spectral function $\alpha^2 F(\omega)$ and phonon DOS at 26, 30, and 60 GPa for β Zr are shown in Fig. 3(b). Logarithmic average phonon frequency $\omega_{\log}$ and the EPC

10

TABLE III: Calculated logarithmic average of vibrational frequencies $\omega_{\log}$ and EPC constant λ of α, ω, and β Zr at different pressures.

Phase	Pressure (GPa)	$\omega_{\log}$ (K)	λ
α	0	142.52	0.8611
	5	139.26	0.8852
ω	0	168.29	0.6723
	10	182.27	0.6753
	20	186.51	0.7302
	30	184.06	0.8174
β	26	80.91	2.5311
	28	123.43	2.0237
	30	136.22	1.7822
	40	169.17	1.2745
	50	198.83	1.0147
	60	221.55	0.8528

strength λ of α, ω, and β Zr at different pressures are listed in Table III. The superconducting T_c has been estimated from Eqs. (3), and a typical value of Coulomb pseudopotential μ^*=0.12 is used. Our calculated T_c, together with $N(E_F)$, as a function of pressure for the three phases are plotted in Fig. 5. Note that there are two different kinds of atoms for ω Zr: Zr1 in 1a and Zr2 in 2d sites. Clearly, the predicted T_c is in good agreement with experimental results. As indicated by McMilan equation [Eqs. (3)], T_c has tight relationship with $\omega_{\log}$, λ, and $N(E_F)$. From 0-7 GPa, total $N(E_F)$ of α phase increases with pressure. In pressure range of 7-30 GPa, the average $N(E_F)$ of ω phase over two kinds of atomic arrangements also exhibits increasing behavior upon compression. In contrast, total $N(E_F)$ of β Zr decreases with pressure in the whole domain of 26-60 GPa. All these pressure-dependent behaviors of $N(E_F)$ obey one known fact that a more stable phase has a lower value of $N(E_F)$. Through plotting partial $N(E_F)$ of s, p, and d orbitals (not shown), we find that the main contribution to the pressure-dependent behavior of the total $N(E_F)$ comes from d orbital. The s orbital has no contribution and the contribution from p orbital is limited.
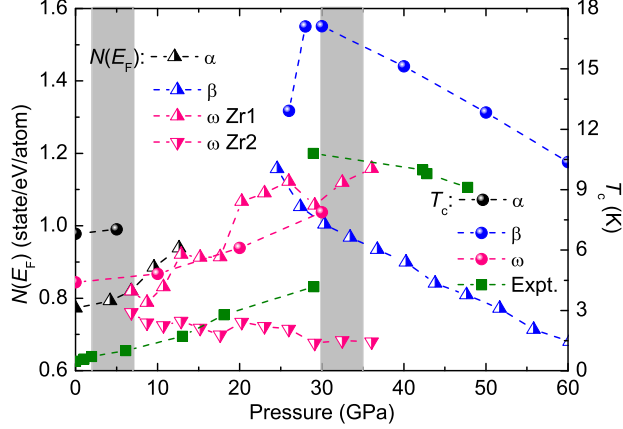
FIG. 5: (Color online) Calculated total density of state at the Fermi level $N(E_F)$ and superconducting transition temperature T_c as functions of pressure for α, ω, and β Zr. The experimental values of T_c from Ref. [9] are also presented. The two shaded regions indicate the $\alpha \to \omega$ and $\omega \to \beta$ phase transition ranges of $2-7$ GPa [5–7] and $30-35$ GPa [6, 8–11], respectively.

From Fig. 5, one can see that the experimental T_c changes in almost the same way as that of the $N(E_F)$. So, it seems that relative larger value of the $N(E_F)$ for β Zr at 26 GPa may predict larger T_c for superconductivity. However, $N(E_F)$ is less directly important than $\omega_{\log}$ and λ for T_c.

From Table III, one can see that the calculated λ for α and ω phases increases with pressure while $\omega_{\log}$ does not show any clear dependence on pressure. As a result, the increasing behavior of T_c upon compression is mainly due to the increase of λ. For β Zr, $\omega_{\log}$ and λ have an almost opposite evolution with pressure. However, the changing rate for $\omega_{\log}$ and λ is different. The increasing rate of $\omega_{\log}$ is clearly larger than the decreasing rate of λ in pressure range of 26 to 30 GPa. After being compressed over 30 GPa, the decreasing rate of λ exceeds the increasing rate of $\omega_{\log}$. So the main affection to the pressure performance of T_c comes from the increase of $\omega_{\log}$ in pressure domain 26-30 GPa, while in 30-60 GPa is from the decrease of λ. Therefore, the relatively small value of T_c at 26 GPa for β Zr is understandable. Furthermore, the lowest transverse-acoustics (TA1) soft mode for bcc β Zr in pressure range of 26-30 GPa is evident [Fig. 3(b)] and can lead a significant electron-phonon contribution. Therefore, as indicated in Table III, the EPC constant λ at 26-30 GPa is predominantly larger than that of both α and ω phases. And, along with increasing the pressure, soft vibrational mode for β Zr gradually fade away, resulting in the decrease of λ

and T_c. Thus, the decrease of λ and T_c for β Zr under pressure mainly originates from the fading of soft vibrational modes induced by increasing pressure.

IV. CONCLUSION

In summary, the elasticity, dynamic properties, and superconductivity of Zr under pressure up to 60 GPa have been studied by means of the first-principles DFT-PBE method. Our results have shown that the structural parameters, elastic constants, elastic moduli, Poisson's ratio, ultrasonic velocities, and Debye temperature of α and ω phases coincide well with experiments. The $\alpha\rightarrow\omega$ and $\omega\rightarrow\beta$ phase transition pressures at $T=0$ K have been calculated to be -3.7 GPa and 32.4 GPa, respectively. The compression curve of β Zr is well consistent with experiments. Our calculations have explicitly indicated that the low elastic modulus of Zr occurs at low pressure in β phase.

In phonon dispersion study, the soft modes of β phase along [111] and [110] directions have been shown and the $\beta\rightarrow\omega$ and $\beta\rightarrow\alpha$ transition paths have been predicted. Dynamic stability test has illustrated that β Zr is unstable till being compressed over 25 GPa. In addition, superconductivity has been obtained by electron-phonon coupling calculations and our calculated T_c accords well with experiments. Through analyzing the electronic density of states at the Fermi level, we have derived that the main contribution to the pressure-dependent behavior of the superconductivity comes from the d orbital. The large T_c at around 30 GPa for β Zr is mainly due to the TA1 soft mode. Under pressure, the increase or decrease of T_c for Zr in all three phases has tight relation with the corresponding behavior of the EPC constant λ.

---

[1] H. Ikehata, N. Nagasako, T. Furuta, A. Fukumoto, K. Miwa, and T. Saito, Phys. Rev. B **70**, 174113 (2004).

[2] W. Liu, B. Li, L. Wang, J. Zhang, and Y. Zhao, Phys. Rev. B **76**, 144107 (2007).

[3] M. T. Pérez-Prado and A. P. Zhilyaev, Phys. Rev. Lett. **102**, 175504 (2009).

[4] Q. M. Hu, S. J. Li, Y. L. Hao, R. Yang, B. Johansson, and L. Vitos, Appl. Phys. Lett. **93**, 121902 (2008).

[5] S. K. Sikka, Y. K. Vohra, and R. Chidambaram, Prog. Mater. Sci. **27**, 245 (1982).

[6] H. Xia, S. J. Duclos, A. L. Ruoff, and Y. K. Vohra, Phys. Rev. Lett. **64**, 204 (1990).

[7] Y. S. Zhao, J. Z. Zhang, C. Pantea, J. Qian, L. L. Daemen, P. A. Rigg, R. S. Hixson, G. T. Gray III, Y. P. Yang, L. P. Wang, Y. B. Wang, and T. Y. Uchida, Phys. Rev. B **71**, 184119 (2005).

[8] H. Xia, A. L. Ruoff, and Y. K. Vohra, Phys. Rev. B **44**, 10374 (1991).

[9] Y. Akahama, M. Kobayashi, and H. Kawamura, J. Phys. Soc. Jpn. **59**, 3843 (1990).

[10] Y. Akahama, M. Kobayashi, and H. Kawamura, J. Phys. Soc. Jpn. **60**, 3211 (1991).

[11] Y. S. Zhao and J. Z. Zhang, Appl. Phys. Lett. **91**, 201907 (2007).

[12] P. E. Blöchl, Phys. Rev. B **50**, 17953 (1994).

[13] G. Kresse and J. Furthmüller, Phys. Rev. B **54**, 11169 (1996).

[14] J. P. Perdew, K. Burke, and M. Ernzerhof, Phys. Rev. Lett. **77**, 3865 (1996).

[15] H. J. Monkhorst and J. D. Pack, Phys. Rev. B **13**, 5188 (1972).

[16] A. D. C. S. Baroni, S. de Gironcoli, P. Giannozzi, C. Cavazzoni, G. Ballabio, S. Scandolo, G. Chiarotti, P. Focher, A. Pasquarello, K. Laasonen, A. Trave, R. Car, N. Marzari, and A. Kokalj, http://www.pwscf.org.

[17] S. Baroni, P. Giannozzi, and A. Testa, Phys. Rev. Lett. **58**, 1861 (1987).

[18] P. Giannozzi, S. de Gironcoli, P. Pavone, and S. Baroni, Phys. Rev. B **43**, 7231 (1991).

[19] F. Birch, Phys. Rev. **71**, 809 (1947).

[20] R. Hill, Phys. Phys. Soc. London **65**, 349 (1952).

[21] P. B. Allen and R. C. Dynes, Phys. Rev. B **12**, 905 (1975).

[22] W. L. McMillan, Phys. Rev. **167**, 331 (1968).

[23] Y. J. Hao, L. Zhang, X. R. Chen, L. C. Cai, Q. Wu, and D. Alfè, Phys. Rev. B **78**, 134101 (2008).

[24] I. Schnell and R. C. Albers, J. Phys.: Condens. Matter **18**, 1483 (2006).

[25] C. S. Barrett and T. B. Massalski, *Structure of Metals* (New York: McGraw-Hill, 1966).

[26] A. Heiming, W. Petry, J. Trampenau, M. Alba, C. Herzig, H. R. Schober, and G. Vogl, Phys. Rev. B **43**, 10948 (1991).

[27] E. A. Brandes, *Smithells Metals Reference Book* (Butterworth, London, 1983).

[28] Y. J. Hao, L. Zhang, X. R. Chen, Y. H. Li, and H. L. He, J. Phys.: Condens. Matter **20**, 235230 (2008).

[29] R. Ahuja, J. M. Wills, B. Johansson, and O. Eriksson, Phys. Rev. B **48**, 16269 (1993).

[30] W. Liu, B. Li, L. Wang, J. Zhang, and Y. Zhao, J. Appl. Phys. **104**, 076102 (2008).

[31] P. Souvatzis, O. Eriksson, M. I. Katsnelson, and S. P. Rudin, Phys. Rev. Lett. **100**, 095901 (2008).

[32] Z. G. Mei, S. L. Shang, Y. Wang, and Z. K. Liu, Phys. Rev. B **80**, 104116 (2009).